IIETA International Information and Engineering Technology Association
Advancing the World of Information and Engineering

Journal of New Materials for Electrochemical Systems
Vol.22, No.4, October, 2019, pp. 224-230
http://new-mat.org
http://iieta.org/journals/jnmes

Study on Preparation of Eco-friendly Autoclaved Aerated Concrete from Low Silicon and High Iron Ore Tailings

Xiaoying Liang[1,2], Changlong Wang[2,3,4]*, Jiayu Zhan[1]*, Xiaowei Cui[5] and Zhenzhen Ren[1]

[1]State Key Laboratory of Solid Waste Reuse for Building Materials, Beijing Building Materials Academy of Science Research, Beijing 100041,China;
[2]School of Civil Engineering, Hebei University of Engineering, Handan Hebei Province, 056038, China;
[3]Jiangxi Key Laboratory of Mining Engineering, Jiangxi University of Science and Technology, Ganzhou Jiangxi Province 341000, China;
[4]Tianjin Sunenergy Sega Environmental Science & Technology Co. Ltd, Tianjin 300000, China;
[5]Shaanxi Key Laboratory of Comprehensive Utilization of Tailings Resources, Shangluo University, Shangluo Shaanxi Province 726000, China

Corresponding Author Email: baistuwong@139.com; zhanjiayu1981@126.com

ABSTRACT

In order to realize the resource utilization of solid waste, autoclaved aerated concrete (ACC) was prepared with low silicon and high iron tailings (IOT) as the main siliceous materials. The effects of fineness and content of siliceous materials, and static curing temperature on the AAC properties, hydration products and microstructures of AAC were investigated by physical and mechanical properties test, X-ray diffraction analysis (XRD), and scanning electron microscope (SEM). The result shows that the AAC containing 40% IOT (in mass percentage) with a specific surface area (SSA) of 311 $m^2 \cdot kg$-1 can achieve a compressive strength of 4.15 MPa and bulk density of 587 $kg \cdot m^{-3}$, which qualifies the requirements of B06, A3.5 of AAC sample regulated by the composition and morphology GB/T 11969-2008. And the main phases in the system contain hydration products, ferrotschermakite, hornblende, anhydrite, calcite, dolomite and residual quartz. The main hydration products are 0.9 nm, 1.1 nm and 1.4 nm tobermorite and C-S-H gels. And the strength mainly results from cementation between hydration products tobermorite and C-S-H gels and unreacted components.

Keywords: *iron ore tailings, autoclaved aerated concrete, fineness, content, tobermorite*

Received: August-04-2019, Accepted: October-15-2019, https://doi.org/10.14447/jnmes.v22i4.a08

1. INTRODUCTION

Iron ore tailings (IOT) are the industrial solid waste from iron separation. With the rapid development of the steel industry, the proportion of the IOT in the industrial solid waste industry has been also increasing. There are more than 400 large-scale tailings dams in China, among which the tailings impoundment from metal mines reaches over 6 billion tons. At present, tailings are still growing at a rate of 300 million tons per year, with the IOT accounting for 1/3 of them [1-3]. Therefore, whether it is used as a secondary resource or a source of pollution, the IOT have been one of the key research topics of mining enterprises, universities and research institutes. The comprehensive utilization of tailings in China mainly focuses on the extraction of valuable elements [4, 5], the production of construction materials [6-11], and the use as filling materials [12, 13]. In recent years, the IOT have been used as new siliceous materials to prepare the autoclaved aerated concrete (AAC). Li et al. [14] used Miyun IOT to prepare the AAC products with a content of 62% and a compressive strength of 6 MPa; however, the siliceous materials used were high-silicon low-iron tailings, and the process cannot meet the requirements for preparing the AAC product with low-silicon, high-iron, and silicate-rich tailings, resulting in a low rate of achievement transformation and promotion rate. Based on the related research results, this paper attempts to study the preparation of the AAC using the low-silicon and high-iron tailings. For this, taking the low-silicon high-iron-type silicate-rich tailings as the main raw material, it explores the basic process of preparing the AAC through the iron ore tailings-silica sand-cement-lime raw material system, and analyses the effect of the fineness of raw materials, mixing amount, and static curing time on the AAC performance. Also, testing methods of X-ray diffraction analysis (XRD), and scanning electron microscope (SEM) were used to study the hydration products types and micro-morphology of the AAC.

2. MATERIALS AND METHODS

2.1 Materials

(1) IOT. The IOT from Shanxi Lingqiu Haoyang Mining Co., Ltd was precipitated, dried, mixed, and reduced during the mine separation process of the comprehensive tailings in the ore dressing plant, to obtain the representative research samples in this study. The results of phase analysis (Fig. 1) show that the main phases of the IOT are composed of quartz, hornblende, grunerite, and plagioclase, as well as rare biotite, chlorite, and calcite; the main chemical composition of the IOT include SiO_2, Al_2O_3, Fe_2O_3, and FeO; the Fe content in the tailings is relatively high, and the total iron content TFe is 14.51% (Table 1); also, the IOT studied are high-iron, low-silicon, and iron silicate-rich. Because the SiO_2 content in the iron tailings of 54.41% do not meet the requirement in the AAC production, it's necessary to add silica

Table 1. Chemical composition of raw materials (mass fraction, %)

Materials	SiO_2	Al_2O_3	Fe_2O_3	FeO	MgO	CaO	Na_2O	K_2O	SO_2	Loss
IOT	54.41	7.99	8.94	10.65	5.75	5.06	0.98	0.43	1.26	2.90
SS	87.07	5.87	0.64	0.19	0.97	1.34	1.00	1.90	—	0.93
Lime	5.45	3.85	1.68	0.08	3.59	78.76	—	1.25	0.45	3.93
OPC	25.06	6.10	3.31	0.21	3.87	55.56	0.23	0.95	—	4.16
FGDG	2.84	0.78	0.25	0.03	0.47	40.13	0.14	0.12	33.21	—

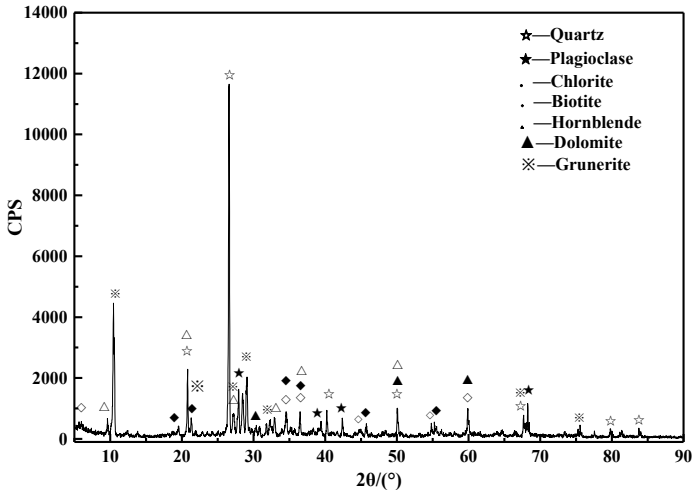

Figure 1. XRD spectra of IOT

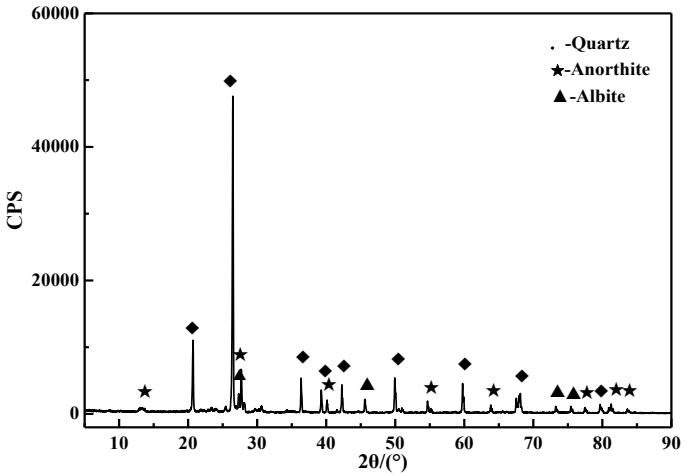

Figure 2. XRD spectra of the SS

sand with a higher SiO_2 content as the siliceous materials.

(2) Silica sand (SS). Using the aeolian sand in industrial production. Its chemical composition is shown in Table 1. The XRD analysis results are shown in Fig. 2. It can be seen from Table 1 that the SiO_2 content of SS reached 87.17%, satisfying the requirements for use. Fig. 2 shows a high content of quartz in the SS used in the test.

(3) Lime. Using the commercial quick lime, with the fineness controlled about 0.08 mm, and square hole sieve with less than 15% sieve. After testing, its effective CaO content is 74%, MgO content is 3.59%, SiO_2 is 5.45%, digestion time is 13min, and digestion temperature is 66 °C, in line with the requirements of the national standard JC/T 621-2009 *Lime for Silicate Building Products*. Its chemical composition is shown in Table 1.

(4) Ordinary Portland cement (OPC). The commercially available P.O 42.5 ordinary Portland cement. Its chemical composition is shown in Table 1. The initial setting time of the cement is 118 minutes and the final setting time is 390 minutes, in line with the quality requirements of cement in GB 175-2007 *Common Portland Cement*.

(5) Flue Gas Desulfurization gypsum (FGDG). It's from Beijing Jingneng Power Co., Ltd., with 8% residue on 0.08 mm square-hole sieve. Its chemical composition is shown in Table 1.

(6) Aluminium powder. FQ-80B type hydrophilic Al powder is used in the test. Its active Al content is 92%, the 2.6% residue on the 0.08mm square hole sieve, the aeration rate is greater than 80%, the aeration time is less than 24 minutes, and the hydrophilicity is less than 20 seconds.

2. 2 Methods

The IOT and SS were first dried to a moisture content of less than 1%, and then placed in a 5 kg laboratory ball mill (SMφ500 mm × 500 mm) for grinding. The rotation speed of the mill was 48 $r \cdot min^{-1}$, the grinding medium was steel balls and steel forging, and the loading capacity of the grinding medium was 100 kg. Among them, the steel ball was 60 kg; the quality gradation was φ70 mm accounting for 19.7%, φ60 mm 33.1%, φ50 mm 29.6%, and φ40 mm 17.6%; steel forging was 40 kg, φ25 mm × 30 mm in size. The purpose of this study is to prepare A3.5, B06-class AAC products adopted with the IOT. After the ratio optimization test, the basic formula of the raw materials was determined. Based on this, the AAC performance was tested according to the national standard using a 100 mm × 100 mm × 100 mm test mould. The process of sample preparation is as follows: according to the mixing ratio, mix the ground iron tailings and SS with lime, cement, and FGDG, and add warm water at 55 °C for 90 s; then add aluminium paste and stir for 40 s. After pouring, static curing, demoulding, autoclaving process, the AAC samples were finished. The ambient temperature of aeration and static curing was 40~70 °C. After 4 hours of static curing, the strength of the test sample can meet the requirements of the cutting process in production. In this test, the forming and pre-curing of the test pieces were completed in the laboratory, and then the green body was transported to the factory for saturated steam pressure autoclaving using an industrial autoclave. The autoclaving system was: temperature rise for 2 hours, constant temperature for 8 hours (maximum pressure 1.25 MPa, and temperature 185 °C), temperature reduction for 2h for obtaining the AAC products.

2.3 Characterization of the AAC properties

This study aims to produce the AAC products doped with the IOT with a volume mass of 600 $kg \cdot m^{-3}$ (B06 class). In the test, the physical and mechanical properties of such AAC products were measured in accordance with the national standard *Test methods of autoclaved aerated concrete* (GB/ T11969-2008)". When testing the compressive strength and bulk density, the moisture content of the product was controlled to 8%~12%.

CZB-9 automatic specific surface area meter (SSA) was used to

Table 3. The influence of different fineness of IOT on pouring stability and AAC properties

Number	SSA /($m^2 \cdot kg^{-1}$)	Slurry fluidity	Pouring stability	Bulk density /($kg \cdot m^{-3}$)	Compressive strength/MPa
T1	225	poor	bubble	620	1.83
T2	244	poor	bubble	612	1.98
T3	286	general	good	603	2.05
T4	311	good	good	595	2.41
T5	345	good	better	596	2.35
T6	385	good	better	608	2.18
T7	429	better	slight bubble	623	2.14

measure the SSA of the ground raw materials; YES-300 digital display and hydraulic pressure testing machine was adopted to test the mechanical properties, with the maximum load of 300KN, and the loading rate of (2.0 ± 0.5) kN/s; a Rigaku D/MAX-RC 12KW XRD was applied to analyse the AAC samples, Cu target, with a wavelength of 1.5406 nm, a working current of 150mA, and a working voltage of 40 kV; Zeiss SUPERTM[55] field emission Scanning electron microscope (FE-SEM) was used to observe the morphology of hydration products in the AAC samples.

3. RESULTS AND DISCUSSION

3.1 Effect of IOT fineness on the AAC properties

The grinding time of the IOT and SS is a key factor in the preparation of the AAC. The size of IOT and SS particles directly affects the stability of slurry casting and the level of the AAC reaction activity. Studies have shown that when the product system cured by autoclaving is mixed with ground IOT and SS, the crystalline silica in the system has the conditions to participate in the hydration reaction. The ground IOT and SS not only has a filling effect, but also can cause substantial chemical reactions to generate the main phases of the AAC. The IOT and SS used in the test were relatively low in activity. To be used as a cementing material in the AAC, they must first be activated. The reaction activation energy of materials is decreased through mechanochemical effects [15-17]. The mechanical force reduces the particle size of the raw material particles, increases the SSA, and generates many new surfaces. With the surface free energy increasing, the reactivity also increases.

3.1.1 Determination of IOT fineness

The residue on 0.08 mm square hole sieve of the raw IOT is 70.80%, which cannot be directly used to produce the AAC. They should be ground and homogenized by a ball mill. The grinding time and the corresponding SSA are shown in Fig. 3.

The AAC was prepared from IOT of different grinding fineness, and the casting stability and product properties were tested to determine the grinding fineness of the IOT. The main raw material ratio (mass percentage) in the test tentatively determined in this test was: IOT 60%, OPC 12%, lime 23%, FGDG 5%, water and aluminium powder consumption for 58% and 0.06% of the total dry materials, mixing temperature 55 °C, and curing temperature 55 °C. Table 3 shows the influence of the IOT with different fineness on the AAC performance under the same test conditions.

Table 3 The influence of different fineness of IOT on pouring stability and AAC properties

Table 3 shows that the effect of the IOT fineness on its reactivity plays a vital role in the stability of the slurry. As with cementitious materials such as cement, improving the fineness can increase SSA of

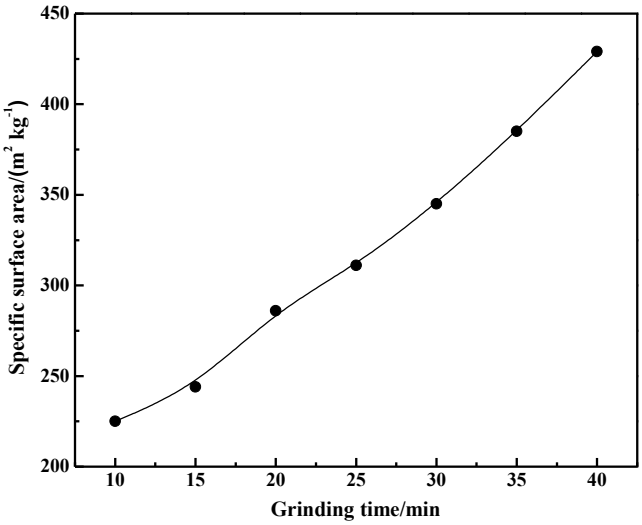

Figure 3. Relationship between grinding time and SSA of IOT

the IOT in contact with water. As a result, the new surface crystals are ground and broken, and become amorphous, which increases the dissolution rate, and enhances the ability of materials to participate in chemical reactions, thereby stimulating the activation of the IOT. The finer the IOT, then the larger the SSA of the particles participating in the reaction, the higher the activity, the better the fluidity of the slurry, but at the same time, it is easy to cause the slurry to be too thick, resulting in insufficient aeration. When the IOT powder is ground to below dozens of microns, it shall fail to provide a good framework structure for the product, resulting in a poor pore structure, which is consistent with the conclusions obtained by observing the appearance effect of the AAC samples. The IOT have coarse particles, poor slurry fluidity, fast settlement after pouring, and are liable to cause mould collapse and subsidence. The results of this test prove that as the grinding time of the IOT increases, the compressive strength of the sample increased first and then decreased; when the grinding for 25 minutes, the enhancement effect reaches the maximum value, and the AAC sample looks the best. Therefore, considering the economic and performances, the SSA of the tailings during the subsequent tests was determined to be 311 $m^2 \cdot kg^{-1}$ (grinding time 25 min).

If the low-silicon and high-iron tailings used in this test were not doped with siliceous materials, it would have been difficult to produce samples meeting the requirements of A3.5 and B06-class qualified products. Thus, high-silica materials such as SS at reasonable ratio should be added to improve the SiO_2 required for the reaction, provide the aggregate of the skeleton required by the product, and find out the optimal point between the IOT and the SS, thereby improving the overall strength of the AAC samples.

3.1.2 Determination of silica sand fineness

The residue on 0.08 mm square hole sieve of the original SS is 30.21%. The grinding time of SS and the corresponding SSA are shown in Fig. 4.

The AAC was prepared from SS with different SSA. The amount of SS used in the test was 60%, while the amount of the other raw materials and curing conditions were the same as those of the AAC with different fineness. Table 4 shows the influence of SS with different fineness on the performance of the AAC under the same test conditions.

Table 4 shows that the bulk density and compressive strength of the samples increased significantly with the extension of the SS grinding time. The compressive strength of the AAC sample was the maximum under the premise of the fine grinding for 35 minutes. When grinding

Table 4. The influence of different grinding time of SS on pouring stability and AAC properties

Number	SSA /($m^2 \cdot kg^{-1}$)	Slurry fluidity	Pouring stability	Bulk density /($kg \cdot m^{-3}$)	Compressive strength/MPa
S1	187	poor	bubble	575	3.04
S2	199	poor	bubble	582	3.14
S3	221	general	better	588	3.41
S4	276	good	better	588	3.60
S5	334	good	good	591	4.46
S6	348	good	good	594	4.51
S7	387	better	slight bubble	598	4.37

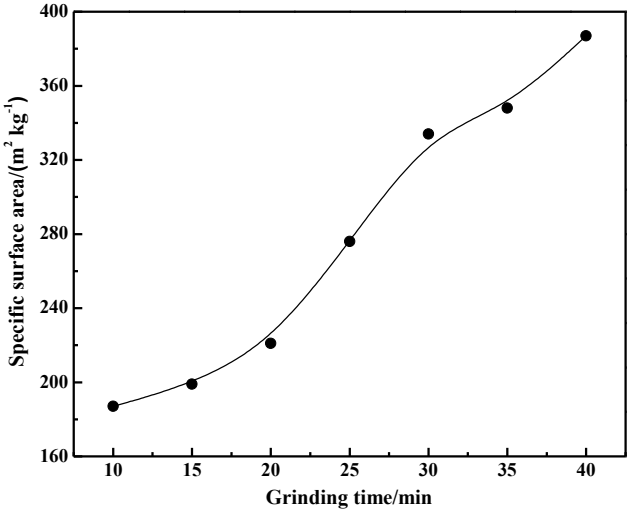

Figure 4. Relationship between grinding time and SSA of SS

time was continued, the compressive strength of the sample was reduced. From the surface of the sample, when the SS grinding time is short, it shall result in coarse SS particles, small contact surface with the slurry quicklime, insufficient reaction, poor workability of the slurry, and the liability to produce honeycomb phenomenon. On the contrary, the long grinding time of SS can lead to a small amount of aggregate, the lack of the proper skeleton in the product, and increase the shrinkage value of the AAC sample, which easily causes the cracks to appear around the AAC sample, and is not conducive to use. When grinding the SS for 35 minutes, the slurry fluidity and pouring stability are good, but large cracks may appear on the outer surface of the product perpendicular to the aeration direction. Therefore, considering the pouring stability, product performance, grinding energy consumption, economy and other factors, it's determined that the grinding time of SS was 30 minutes (SSA: 334 $m^2 \cdot kg^{-1}$).

3.2 Effect of IOT content on the AAC properties

IOT with a fineness of 311 $m^2 \cdot kg^{-1}$ and SS with a fineness of 334 $m^2 \cdot kg^{-1}$ were used for the admixture test. In the test the amount of FGDG used as a regulator was tentatively set at 5%, while the other test conditions were the same as that of the fineness testing: the mixing amount of the IOT was selected to be 30%, 35%, 40%, 45%, 50%, and 55% respectively in order to maximize the use of the IOT; the content of SS was 5%, 10%, 15%, 20%, and 25%, and 30% respectively, lime content was 20%, 25%, 30%, and OPC content was 5%, 10% 15%, aluminium paste 1.32 g, water 1276 g, mixing temperature 55°C of warm water, static curing temperature of 55 °C. Thus, according to the low-to-high calcium-silicon ratio, and low-to-high cement-lime ratio, the test plan was designed to study the influence of the IOT content on the AAC properties. Table 5 shows the mix ratio and physical and mechanical properties of the main raw materials.

The data in Table 5 shows that with the OPC content of 10% and 15%, and the lime content of 20% and 25%, the compressive strength of the product was higher. With the purpose to maximize the use of the IOT and reduce costs of the product, the mixing ratio of A8 products was selected to be the optimal one, i.e., the amounts of the IOT, SS, lime, OPC, and FGDG are 40%, 20%, 25%, 10%, and 5%.

Under the condition of the same raw material mixture ratio, the different static curing temperature shall cause the speed of slurry thickening after casting to vary. Also, the speed of slurry thickening is not completely coordinated with the aeration speed of aluminium paste. In order to acquire the best product performance, it is necessary to keep the speed of the two synchronized, which is conducive to the formation of a better pore structure in the moulding of the product, and to ensure that the product obtains better strength after autoclaving. This test used A8 ratio to test the effect of curing temperature on the AAC performance. The test results are shown in Table 6.

It can be seen from Table 6 that when the static curing temperature was 40~60 ºC, the compressive strength and specific strength of the AAC samples increased; when it was 60~70 ºC, the compressive strength decreased; at a curing temperature of 60 ºC, the AAC product had the highest compressive strength, reaching 4.20 MPa. This indicates that the increase of the static curing temperature is beneficial to the strength development of the product, but the high temperature can cause the water to vaporizes too quickly during the moulding process of the product, resulting in inconsistency between the slurry thickening speed and the aluminium

Table 5. The effect of different content of IOT on AAC properties

Number	Ratio of raw materials (%)					Bulk density /($kg \cdot m^{-3}$)	Compressive strength/MPa
	IOT	SS	Lime	OPC	FGDG		
A1	30	30	20	15	5	604	4.16
A2	30	30	25	10	5	596	4.10
A3	30	30	30	5	5	590	4.05
A4	35	25	20	15	5	593	4.18
A5	35	25	25	10	5	591	4.17
A6	35	25	30	5	5	587	4.09
A7	40	20	20	15	5	592	4.17
A8	40	20	25	10	5	587	4.15
A9	40	20	30	5	5	582	4.10
A10	45	15	20	15	5	598	4.14
A11	45	15	25	10	5	590	4.11
A12	45	15	30	5	5	588	4.06
A13	50	10	20	15	5	599	3.84
A14	50	10	25	10	5	593	3.79
A15	50	10	30	5	5	588	3.64
A16	55	5	20	15	5	602	3.45
A17	55	5	25	10	5	598	3.39
A18	55	5	30	5	5	595	3.25

Table 6. The influence of static curing temperature on AAC properties

Number	Curing Temperature / ºC	Bulk density /(kg·m^{-3})	Compressive strength/MPa
C1	40	593	3.85
C2	45	590	4.02
C3	50	591	4.12
C4	55	587	4.15
C5	60	588	4.20
C6	65	590	4.17
C7	70	586	4.09

paste aeration speed, non-smooth aeration, and even the gas blockage, which is not good for the strength development of the product after autoclaving. Therefore, 60 ºC was selected as the best static curing temperature.

3.4 Analysis of hydration products

3.4.1 Phase analysis of AAC sample

XRD was used to analyse the composition of the AAC samples. It qualitatively analysed various hydrated minerals formed mainly of calcium silicate, and their types; semi-quantitatively analyse the amount of production, which has a decisive influence on the performance of the AAC. Fig. 5 shows the XRD spectra of the AAC samples under the optimal mixture ratio of various factors.

It can be seen from Fig. 5 that the main phases in the AAC samole after autoclaving were 0.9 nm tobermorite ($Ca_5Si_6O_{18}H_2$), 1.1 nm tobermorite ($Ca_5Si_6O_{17}\cdot 5H_2O$) and 1.4 nm tobermorite ($Ca_5Si_6O_{18}H_2\cdot 8H_2O$), quartz, ferrotschermakite, hornblende, anhydrite, calcite, and dolomite. During the autoclaving process of the sample, as the SiO_2 in the IOT and siliceous raw materials continuously dissolved, it reacted with calcareous materials such as lime to form the hydrated product-tobermorite. A variety of water bound tobermorite was formed, which may be related to the composition of the AAC products (including water moisture) and the heterogeneity of particle size. Its formation indicates the coexistence of tobermorite with different bound water content in nature [18]. The ferrotschermakite $Ca_2Fe_3Al_2(Si_6Al_2)O_{22}(OH)_2$ in the product has a double-chain structure. Due to the addition of active CaO and Al powder in the sample, Ca^{2+} and Al^{3+} were ion-exchanged with Fe^{2+} and Si^{4+} in amphibole ($Fe_7Si_8O_{22}(OH)_2$) to form ferrotschermakite under high temperature steam curing conditions [19]. In the XRD pattern of the finished sample, anhydrite was generated, which was the residue after the reaction of FGDG in the system, while calcite was caused by the carbonization of the sample.

In the raw tailings such as the dolomite and hornblende, their characteristic peaks in the samples still existed after autoclaving, which must be due to its low activity under the autoclave conditions used in this system, making it impossible for all to participate in the reaction. The IOT minerals such as plagioclase, chlorite, and biotite were decomposed after autoclaving, entered the tobermorite structure, and form a new mineral phase, which is extremely beneficial to the development of sample strength. By comparing Fig. 1 with Fig. 5, it can be found that the intensity of quartz's diffraction peak was obviously decreased, which indicates that there was some residual after the quartz participat-

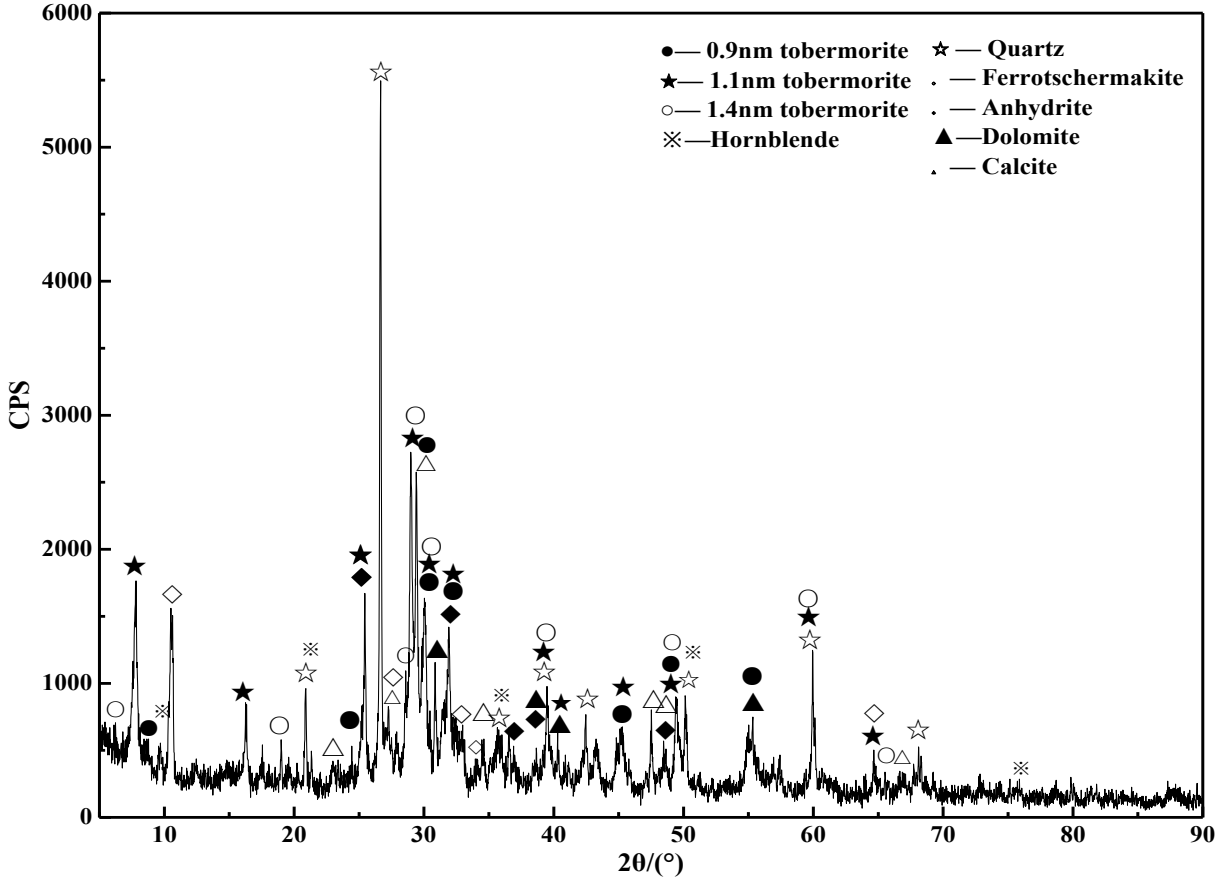

Figure 5. XRD spectra of A8 AAC samples

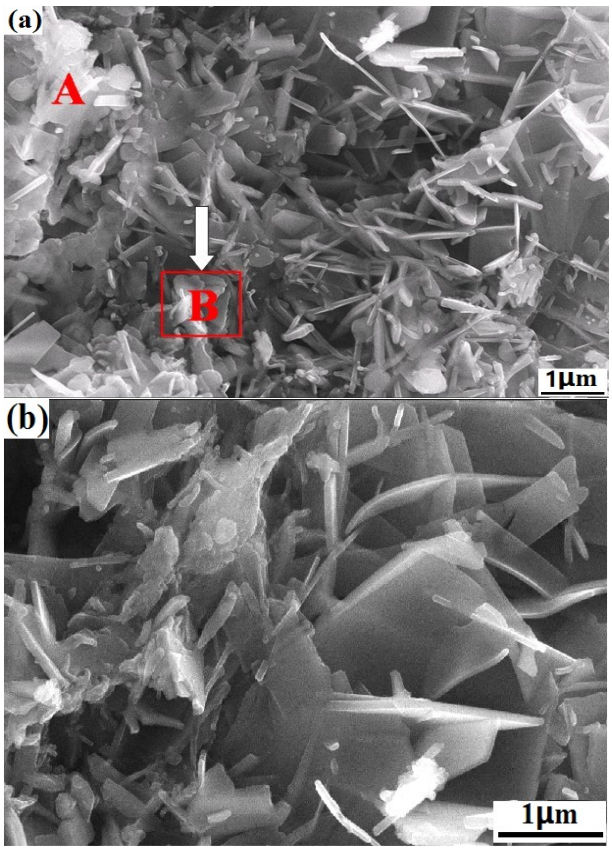

Figure 6. SEM micrographs of A8 AAC sample. (a) 30,000-fold enlargement of hydration products of samples, (b) 50,000-fold enlargement of hydration products of region B in Fig. 6 (a)

ing in the reaction, and the main residual aggregate of quartz existed. In addition, the XRD pattern had a certain dispersed background, which proves that certain amorphous (non-diffractive) substance existed in the sample A8, and there were some small particle sizes in the product, resulting in broadening of the diffraction peaks, and merging into the XRD diffraction background [20].

3.4.2 Analysis for micro-morphology of hydration products

Fig. 6 (a) shows the autoclaved AAC samples, in which the hydration products were densely clustered, and low crystallinity or amorphous C-S-H gels (A in the Fig. 6(a)) and a large amount of well-crystallinity tobermorite in the shape of willow leaf or leaf (B in the Fig. 6(b)) were formed on the sample section; C-S-H gels acted as a "binder" to OPC these dense hydration products together and form a good network-like frame structure, which can change the pore structure of the product, and better resist external loads, and under stress, makes it not easy to cause stress concentration, playing a role in improving the strength of the samples [21-26]. In Fig. 6 (b), it can be seen from the enlarged image of B from Fig. 6 (a) that the hydrated product tobermorite had a good crystal form, and at the same time, and there were unreacted quartz particles around the plate- or flake-shaped material; due to the different choices of the field of view, the number of quartz particles also varied.

3.5 Strength formation mechanism analysis of the AAC samples

The same as that of other types of AAC, the reaction process of the AAC doped with the IOT, SS, OPC, lime include the static curing stage and the autoclaving curing stage under high temperature and pressure.

During the static curing period, hydration of the OPC occurred in the casting slurry and the body, quicklime decomposed, and low crystallinity or amorphous C-S-H gels, $Ca(OH)_2$, and a small amount of calcium sulfoaluminate hydrate were formed. Under the conditions of hot alkali excitation, a small amount of SiO_2 components in IOT and SS began to show chemical activity, and reacted with $Ca(OH)_2$ produced by quicklime digestion to form C-S-H gels, so that the product body obtains early strength and is convenient for handling and cutting.

During the autoclave curing stage, as the temperature increased, more SiO_2 in the IOT and SS accelerated to dissolve, and reacted with $Ca(OH)_2$ to form C-S-H gels, while the dual-alkali silicate in the cement reacted with SiO_2 to form the tobermorite and C-S-H gels. Under high-temperature and high-pressure steaming environment, active ionization interacted with OH^-, and the Si-O and Al-O bonds in the system are broken, which promoted the SiO_2 and Al_2O_3 components in the raw material system to show activity, and combines with $Ca(OH)_2$ to produce the hydration product and form a supersaturated solution. By maintaining enough steaming time, the hydration products were formed, and interweaved into network after crystallization and nucleation, showing gel property. Since some minerals in the IOT and SS participated in the formation reaction of hydration product under high-temperature autoclaving conditions, more C-S-H gels and tobermorite were formed. These hydration products were tightly wrapped on the surface of the coarse iron tailings particles, giving the product strength. Based on the mechanism analysis of the above, it can be found that the strength of the AAC depends on the cementation of the hydration products such as C-S-H gels and tobermorite (formed by the reaction of cement, lime and the active components SiO_2 and Al_2O_3 in the raw materials system) with other ingredients together.

4. CONCLUSIONS

(1) Using low-silicon high-iron-type IOT as the main siliceous materials, qualified products of the AAC in A3.5, B06-class regulated by national standards can be prepared. The optimized ratio is: the specific surface area of iron tailings 311 $m^2 \cdot kg^{-1}$, the mass ratio of IOT, SS, lime, OPC, FGDG 40:20:25:10:5, the water-to-material ratio 0.58, the amount of aluminium powder added to be 0.06% of the total dry material, and the curing temperature of 60 ºC.

(2) XRD and SEM analysis showed that under high-temperature autoclaved conditions, the hydration products of the AAC were a large number of well-crystallized tobermorite in the shaper of willow leaf or leaf with different combined water contents and low-crystallized or amorphous CSH gel; Ca^{2+} and Al^{3+} were ion-exchanged with Fe^{2+} and Si^{4+} in amphibole ($Fe_7Si_8O_{22}(OH)_2$), respectively, to form ferrotschermakite; plagioclase, biotite and chlorite were completely decomposed after participating in the reaction of the system; anhydrite was generated, as the residue of the reacted FGDW in the system, while the calcite was caused by carbonization of the product; dolomite and ordinary amphibole in iron tailings with low activity did not participate in the system reaction; the quartz participated in the system reaction, but leaving some residual particles behind.

(3) The mechanism analysis showed that under high temperature autoclaving conditions, the IOT could show good activity, and the active components SiO_2 and Al_2O_3 in the raw material system have an enhanced ability to participate in chemical reactions; the active components SiO_2 and Al_2O_3 reacted with the cement and lime to form hydration products such as C-S-H gels and tobermorite, which can help to enhance the product strength by cementing together with other components.

5. ACKNOWLEDGMENTS

The authors gratefully acknowledge financial support from China Postdoctoral Science Foundation (2016M602082), supported by Natural Science Foundation of Hebei Province (E2018402119), supported by Natural Science Foundation of Shaanxi Province (2019JLM-49), supported by Shaanxi Science and Technology Benefit People Project (2018ZY-HM-01), supported by Science and Technology Research Project of Higher Education Universities in Hebei Province (ZD2016014, QN2016115), supported by Comprehensive Utilization of Tailing Resources Key Laboratory of Shaanxi Province (2017SKY-WK008), supported by Jiangxi Postdoctoral Daily Fund Project (2016RC30), supported by Jiangxi Postdoctoral Research Project (2017KY19), supported by State Key Laboratory of Solid Waste Reuse for Building Materials (SWR-2019-008).

REFERENCE

[1] Wang X L, Ren R C, Liu Y. Application of DTA in preparation of glass-ceramic made by iron tailings, Procedia Earth and Planetary Science, 2009, 1(1),750-753.

[2] Zhang S, Xue X, Liu X. Current situation and comprehensive utilization of iron ore tailing resources. Journal of Mining Science, 2006, 42(4), 403-408.

[3] Li J, Wang Q, Liu J H, Li P. Synthesis process of forsterite refractory by iron ore tailings. Journal of Environmental Sciences, 2009, 21 (suppl.1), 92-95.

[4] Li C, Sun H H, Bai J, Li L T. Innovative methodology for comprehensive utilization of iron ore tailings: Part 1. The recovery of iron from iron ore tailings using magnetic separation after magnetizing roasting. Journal of Hazardous Materials, 2010, 174(1-3), 71-77.

[5] Li C, Sun H H, Yi Z L, Li L T. Innovative methodology for comprehensive utilization of iron ore tailings: Part 2: The residues after iron recovery from iron ore tailings to prepare cementitious material, Journal of Hazardous Materials, 2010, 174(1-3), 78-83

[6] Chen Y L, Zhang Y M, Chen T J, Zhao Y L, Bao S U. Preparation of eco-friendly construction bricks from hematite tailings. Construction and Building Materials, 2011, 25(4), 2107-2111.

[7] Liu Y S, Du F, Yuan L, Zeng H, Kong S F. Production of lightweight ceramisite from iron ore tailings and its performance investigation in a biological aerated filter (BAF) reactor. Journal of Hazardous Materials, 178(1-3), 999-1006.

[8] Zhao Y L, Zhang Y M, Chen T J, Chen Y L, Bao S U. Preparation of high strength autoclaved bricks from hematite tailings, Construction and Building Materials, 2012, 28(1), 450-455.

[9] Yi Z L, Sun H H, Wei X Q, Li C. Iron ore tailings used for the preparation of cementitious material by compound thermal activation, International Journal of Minerals, Metallury and Materials, 16(3), 355(2009)

[10]Yi Z L, Sun H H, Li C, Sun Y M, Li Y. Relationship between polymerization degree and cementitious activity of iron ore tailings[J]. International Journal of Minerals, Metallury and Materials, 2010, 17(1), 116-120.

[11]Liu S J, Hu Q Q, Zhao F Q, Chu X M. Utilization of steel slag, iron tailings and fly ash as aggregates to prepare a polymer-modified waterproof mortar with a core-shell styrene-acrylic copolymer as the modifier. Construction and Building Materials, 2014, 72, 15-22.

[12]Lu H J, Qi C C, Chen Q S, Gan D Q, Xue Z L, Hu Y J. A new procedure for recycling waste tailings as cemented paste backfill to underground stopes and open pits. Journal of Cleaner Production, 2018, 188, 601-612.

[13]Coussy S, Benzaazoua M, Blanc D, Moszkowicz P, Bussière B. Arsenic stability in arsenopyrite-rich cemented paste backfills: A leaching test-based assessment. Journal of Hazardous Materials, 2011, 185(2-3): 1467-1476.

[14]Li D Z, Ni W, Zhang J W, Wu H, Zhang Y Y. Phase transformation of iron Ore tailings during autoclaved curing. Journal of the Chinese Ceramic Society, 2011, 39(4): 708-713.

[15]Roman A. Buyanova, Victor V. Molchanov, Vladimir V. Boldyrev. Mechanochemical activation as a tool of increasing catalytic activity, Catalysis Today, 2009, 144(3-4), 212-218.

[16]Sydorchuk V, Khalameida S, Zazhigalov V, Skubiszewska-Zięba J, Leboda R, Wieczorek-Ciurowac K. Influence of mechanochemical activation in various media on structure of porous and nonporous silicas, Applied Surface Science, 2010, 257(2), 446-450.

[17]Senneca O, Salatino P, Chirone R, Cortese L, Solimene R. Mechanochemical activation of high-carbon fly ash for enhanced carbon reburning, Proceedings of the Combustion Institute, 2011, 33(2), 2743-2753.

[18]Maeshima T, Nomab H, Sakiyama M, Mitsuda T. Natural 1.1 and 1.4 nm tobermorites from Fuka, Okayama, Japan: Chemical analysis, cell dimensions, ^{29}Si NMR and thermal behavior, Cement and Concrete Research, 2003, 33(10), 1515-1523.

[19]Gittos M F, G. W. Lorimer G F, Champness P E. An electron-microscopic study of precipitation (exsolution) in an amphibole (the hornblende-grunerite system), Journal of Materials Science,1974, 9(2), 184-192.

[20]Bensted J, Barnes P. Structure and performance of cements, 2nd edition[M]. New York: Spon Press, 2002.

[21]Bonaccorsi E, Merlino S., Kampf A R. The crystal structure of tobermorite 14 Å (Plombierite), a C-S-H phase, Journal of the American Ceramic Society, 2005, 88(3), 505-512.

[22]Wang C L, Ni W, Zhang S Q, Wang S, Gai G S, Wang W K. Preparation and properties of autoclaved aerated concrete using coal gangue and iron ore tailings [J]. Construction and Building Materials, 2016, 104: 109-115.

[23]Oh J E, Clark S M, Wenk H R, Monteiro P J M. Experimental determination of bulk modulus of 14 Å tobermorite using high pressure synchrotron X-ray diffraction, Cement and Concrete Research, 2012, 42(2), 397-403.

[24]Huang X Y, Ni W, Cui W H, Wang Z J, Zhu L P. Preparation of autoclaved aerated concrete using copper tailings and blast furnace slag. Construction and Building Materials, 2012, 27(1): 1-5.

[25]Cui X W, Wang C L, Ni W, Di Y Q, Cui H L, Chen L. Study on the reaction mechanism of autoclaved aerated concrete based on iron ore tailings [J]. Romanian Journal of Materials, 2017, 47 (1): 46 -53.

[26]Liang X Y, Yuan D X, Li J, Wang C L, Lin X R, Chang N. Preparation and phase characteristics of autoclaved aerated concrete using iron ore tailings [J]. Romanian Journal of Materials, 2018, 48 (3):381 -387